# Effect of Non-additive Mixing on Entropic Bonding Strength and Phase Behavior of Binary Nanocrystal Superlattices

Isabela Quintela Matos[1] and Fernando Escobedo[1, a)]

[1]*F. Smith school of Chemical and Biomolecular Engineering, Cornell University, Ithaca, New York 14853, USA.*

[a)]Corresponding author: fe13@cornell.edu

**Abstract.**

Non-additive mixing plays a key role on the properties of molecular fluids and solids. In this work, the potential for athermal order-disorder phase transitions is explored in non-additive binary colloidal nanoparticles that form substitutionally ordered compounds; namely, for equimolar mixtures of octahedra+spheres which form a CsCl lattice compound, and cubes+spheres which form a NaCl crystal. Monte Carlo simulations that target phase coexistence conditions were used to examine the effect on compound formation of varying degrees of negative non-additivity created by component size asymmetry and by size-tunable indentations in the polyhedra's facets, intended to allow the nestling of neighboring spheres. Our results indicate that the stabilization of the compound crystal requires a relatively large degree of negative non-additivity which depends on particle geometry and the packing of the relevant phases. It is found that negative non-additivity can be achieved in mixtures of large spheres and small cubes having no indentations and lead to the athermal crystallization of the NaCl lattice. For similarly sized components, athermal

congruent transitions are attainable and non-additivity can be generated through indentations, especially for the cubes+spheres system. Increasing indentation leads to lower phase coexistence free energy and pressure in the cubes + spheres system but has the opposite effect in the octahedra + spheres system. These results indicate a stronger stabilizing effect on the athermal compound phase by the cubes' indentations, where a deeper nestling of the spheres leads to a denser compound phase and a larger reduction in the associated pressure-volume free-energy term.

## 1. INTRODUCTION

Multicomponent nanocrystal superlattices can possess unique crystal structures, size-dependent properties, and (upon etching off one component) high surface-to-volume ratios, providing a versatile platform for potential applications in optical, electronic, magnetic, and catalytic materials.[1–5] However, designing mixtures that can assemble into these superlattices presents the key challenge of requiring the fine-tuning the interparticle interaction strengths, component shapes, composition, and external conditions. [6–11] Previous studies have investigated the interactions driving colloidal mixture assembly and the interplay between enthalpic and entropic forces. [12–16] Typically, substitutionally ordered solids or stoichiometric compounds need a selective interaction between the unlike species since, without a preference for the type of neighboring particles, mixing entropy will tend to favor random mixing and consequently substitutionally disordered solids. To assemble athermal solid compounds, the loss of mixing entropy associated with the arrangement of different components in a well-defined repeating pattern must be outweighed by the gains in packing entropy and the decrease of the pressure×volume ($pV$) contribution to the free-energy (which while an enthalpic effect is sometimes folded into the packing entropy concept). One possible approach to increase the packing entropy gain is to utilize

the entropic lock-and-key attraction of shape-complementary particles that generate a negative non-additive mixing. [17–19] Non-additive mixing is more widely associated with molecular fluids and occurs when the volume of the mixed state is either larger (positive) or smaller (negative) than the sum of the individual components' volumes prior to mixing. At a microscopic level, such mixing non-idealities can be correlated with a cross-interaction mixing rule where the characteristic length "$\sigma$" of the contact distance between two particles A and B differs from the arithmetic average of the characteristic contact lengths for A pairs and B pairs, i.e., $\sigma_{AB} = ((\sigma_{AA} + \sigma_{BB})/2 + \Delta)$ with $\Delta \neq 0$); for spherical sites, this corresponds to a violation of the so-called Lorentz's additivity rule.

In colloidal systems, some examples of non-additive mixing include the depletion effect of polymeric depletants on large colloidal particles as embodied by the Asakura-Oosawa model,[20] the Kumar-Molinero model[21] model of a binary mixture of spherical particles having $\Delta > 0$ that lead to the formation of a wide variety of mesophases, and hard-sphere mixtures with $\Delta < 0$ which form compound solids via congruent melting/freezing (i.e., where the phase transition between isotropic and crystal phases occurs at the same composition). [22] As an application for studying non-additivity in superlattice formation, our group proposed a general rule[15,23,24] to maximize the thermodynamic stability of mixtures of spheres and either cubes or octahedra that are known to form crystals with NaCl and CsCl lattices experimentally.[11] In the case of an equimolar mixture of spheres and flat cubes with not too dissimilar sizes, our previous computational study revealed that the formation of a congruent phase transition occurs only with a strong enough inter-species attraction energy. However, we showed in a subsequent study on the same mixture that by replacing flat cubes by dimpled cubes with high indentation sizes, a congruent transition into a purely athermal crystalline phase was achievable. Furthermore, we correlated the extent of mixing non-additivity of the

components with their ability to stabilize the athermal NaCl phase in equilibrium with the isotropic phase.[25] That computational study demonstrated that the strength of inter-species entropic bonds and the formation of ordered phases can be tuned by modifying the size of concavities on polyhedra facets or the sphere-to-cube ratio so as to reduce the geometric frustration (and enhance space tessellation) in the compound phase.

Our previous study [25] explored only a limited range of component size ratios and hence did not consider cases where the compound could be regarded as an interstitial solid where the smaller component fits snugly into the lattice interstices among the large particles. In this study we hence first fill that gap by exploring how large component size asymmetries may lead to the formation of athermal compounds. We further aim to investigate the effect on the compound formation of nanoparticle 'valence', referring to the number of facets per polyhedron, given that dimpled polyhedra have been experimentally synthesized, including tetrahedra, cubes, and dodecahedra.[26–32] We thus sought to determine if athermal superlattice formation could be replicated in other systems besides that of spheres+dimpled cubes, and whether packing entropy or vibration entropy was more significant in stabilizing the athermal phase. For this purpose, we applied a similar methodology to that used for the cubes + spheres system[25] to a mixture of octahedra + spheres, enhancing the entropic bonds by carving indentations to the octahedra facets where the spheres could partially nestle. These dimples allow the octahedra-sphere contact distance to be closer which can result in negative mixing non-additivity ($\Delta < 0$). We also explored the phase diagram of the octahedra-sphere system as a function of the indentation ratio and size ratio between the components, which are experimentally attainable. By comparing the results of both systems, spheres+cubes and spheres+octahedra, we are able to identify their distinct and common features that modulate the forces driving the formation of athermal compound phases.

The rest of the paper is organized as follows. In Section 2 we describe the models and methodology employed. In Section 3 we present and analyze our main results and in Section 4 we conclude by outlining the main takeaways and an outlook for future work.

## 2. COMPUTATIONAL METHODS

### 2.1. System and force field

The system studied in this work consists of a polyhedron (cube or octahedra) with side $a$ and spheres with diameter $\sigma$, and the model follows a similar parameterization as that of our previous study on indented cubes and spheres.[25] The interaction between like particles is purely repulsive, while unlike particles interact through a square-well potential.

$$U_{11} = U_{22} = \begin{cases} \infty, & \text{if overlap} \\ 0, & \text{otherwise} \end{cases} \quad U_{12} = \begin{cases} \infty, & \text{if overlap} \\ -\varepsilon^*, & r \le r_c\,, \delta \le \delta_c = 0.4 d_f \\ 0, & \text{otherwise} \end{cases} \tag{1}$$

Equation (1) states that if no overlap occurs, an energetic contact $-\varepsilon^*$ ensues between a polyhedron and a sphere if the distance between the centers of the particles ($r$) is within a cutoff distance $r_c$ and the distance between the center of the sphere and the vector extending outward from the center of the octahedra facet and perpendicular to it ($\delta$, see Fig. 1(a)) is less than $\delta_c$. This range of energetic contact is depicted as a green region in Fig. 1(a). In this study, $\delta_c$ is set to 40% of the diameter of the circle inscribed in the polyhedra facet ($d_f$), as shown in Figure 1(a) for the octahedra case, and $r_c$ is set to be the minimum distance between the sphere and the polyhedra plus 15% of the side $a$:

$$r_c = h + \frac{\sigma}{2} + 0.15a \tag{2}$$

Here, $h$ is the radius of the sphere inscribed in the polyhedron, which for the octahedron corresponds to $\sqrt{6}/6a$ and for the cube to half its edge ($a/2$). The extent of indentation is defined by the indentation diameter ($d_h$), whose maximum value corresponds to $d_f = \sqrt{3}/3a$ for octahedra and $d_f = a$ for cubes. The distance $d$ defined in Figure 1(b) should be less than $d_{min}$ which is dependent on $d_h$:

$$d_{min} = h + \frac{1}{2}\sqrt{\sigma^2 - d_h^2} \tag{3}$$

$$\delta_{max} = \frac{d_h}{2} - \sqrt{\frac{\sigma^2}{4} - (d - h)^2} \tag{4}$$

where $\delta_{max}$ defines the maximum $\delta$ that a sphere can have without overlapping with the edge of the polyhedra. The criteria for overlap between the polyhedral and sphere are based on Arvo's algorithm.[33] The overlap check between a sphere and an octahedron was based on finding the distance between a point (i.e., the center of the sphere) and a triangle (i.e., the octahedron's facet closest to the sphere) as described in Ref. [33]. Finally, the overlap between non-convex polyhedra is based on the separating axes theorem[34] with indentation-related modifications explained in more detail in our previous paper.[25] We chose to use dimensionless parameters to characterize the systems of interest as summarized in Table 1.

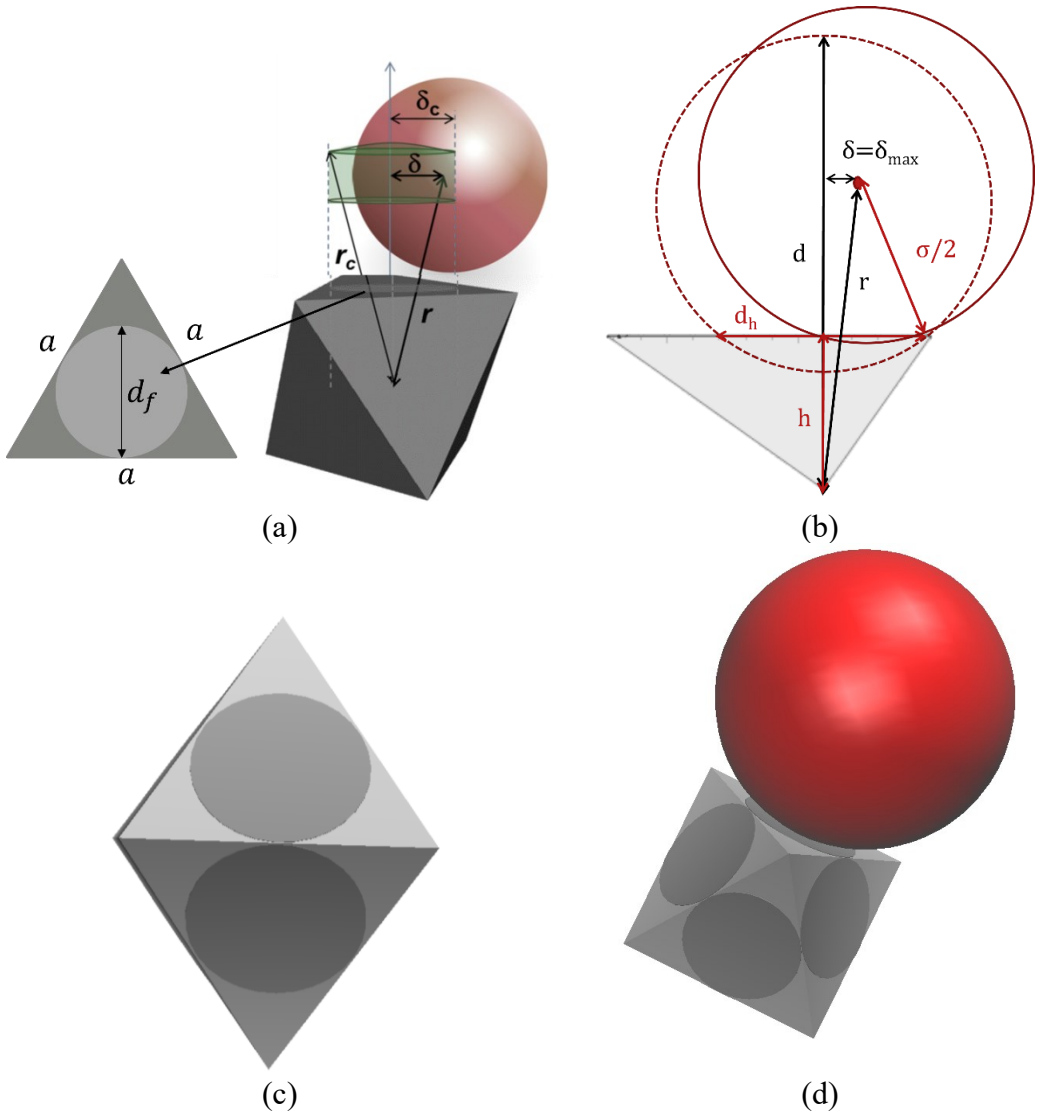


**Figure 1**: (a-b) Schematics of the system geometry and parameters used in criteria for determining overlap for non-convex octahedron (gray) +sphere (red) pairs. The green translucent region in (a) depicts the positions of the sphere's center associated with an energetic contact ($-\varepsilon^*$). (c) Representation of the indentation on octahedra facets. (d) Example of the contact (nestling) of a sphere and an indentation on the octahedron facet.

*Table 1: Design parameters for the spheres + dimpled polyhedra system.*

| Symbol | Meaning | Range for cubes | Range for octahedra |
|---|---|---|---|

| | | | |
|---|---|---|---|
| $\lambda$ | Ratio of indentation diameter ($d_h$) to the polyhedron edge ($a$) | 0.0 – 1.0 | 0.0-0.58 |
| $\zeta$ | Ratio of sphere diameter ($\sigma$) to polyhedron edge ($a$) | 1.19-1.36 | 0.9-1.25 |
| $\varepsilon^*$ | Contact energy between polyhedron and sphere (Eq. (1)) | 0.0 – 1.0 | 0.0-1.5 |

To quantify the extent of non-additivity of our systems, we developed a non-additivity parameter for a binary component system. We utilized the same metric for the non-additivity parameter, $\Delta v$ in Eq. (5), as in our previous study on cubes and spheres.[25] To calculate this parameter in our case, we used the volume of the compound phase, henceforth to be denoted as C*, at infinite pressure (densest state) and the volumes of the densest individual phases of the pure components, namely, the FCC lattice for spheres, the cubic crystal for cubes, and the Minkowski crystal for octahedra:

$$\Delta v = \frac{v(\mathrm{C}^*, p=\infty)}{x_{sph} v(\text{spheres}, p=\infty) + (1-x_{sph}) v(\text{polyhedra}, p=\infty)} - 1 \quad (5)$$

where $x_{sph}$ is the mole fraction of spheres. While $\Delta v$ could be seen as a blunt probe of the tendency for nonadditivty in a C*-forming mixture, unlike the 'microscopic' Lorentz mixing rule, it has the advantage that it can be equally applied regardless of the anisotropy of the NP shapes or interparticle potential shape. We note that in our previous paper[25] the reported $\Delta v$ values were slightly underestimated due to a miscalculation; the correct values for the relevant system (cubes+spheres) are given in the results section 3.5.

### 2.2. Simulations Details

To study the C* (compound) and I (isotropic) phases, we used Monte Carlo (MC) simulations in the isothermal-isobaric ensemble ($N_1N_2PT$). For the C* phase, we started with a perfect CsCl or NaCl lattice, while for the I phase, we used a pre-equilibrated isotropic system. The total number of particles was equal to 1458 for the CsCl phase and 1728 for the NaCl phase with a fixed number ratio of polyhedra to spheres ($N_1 = N_2$). Our simulation results are reported in reduced units: $\varepsilon^* = \varepsilon\beta, v = V/NL^3, p = \beta PL^3,$ and $\rho = NL^3/V$, where the reciprocal temperature $\beta$ is set to 1 and $L$ is equal to $a/\sqrt{2}$ for the CsCl phase of octahedra + spheres and to $a/2$ for the NaCl phase of cubes and spheres.

We traced coexistence lines between the C* phase and the I phase as a function of system design parameters $\lambda$, $\zeta$, and $\varepsilon^*$, defined in Table 1 using the FENEX method. The FENEX method uses a series of polynomials approximations to integrate the equation of the intensive free energy $\phi$:

$$d\phi = zdf + vdp \tag{6}$$

where $v = (\partial\phi/\partial\beta P)_{f,\beta} = V/N$, and $z = (\partial\phi/\partial f)_{\beta P,\beta}$ and $f$ is a field parameter of the system Hamiltonian, i.e. ($f$ =$\lambda$, $\zeta$, or $\varepsilon^*$). The derivative $z$ is evaluated in simulation using a finite perturbation approximation:

$$z \approx -\frac{1}{N\delta f}\ln\frac{\sum\exp[-\beta U(f+\delta f)-\beta PV]}{\sum\exp[-\beta U(f)-\beta PV]} = -\frac{1}{N\delta f}\ln\langle\exp[-\beta U(f+\delta f)+\beta U(f)]\rangle \tag{7}$$

Here, $\delta f$ is a small perturbation on the control variable $f$. If we can decouple $f$ from $U$ (i.e., $\beta U(f) = fU$ ), as for the case when $f = \varepsilon^*$, Eq. (7) can be written as:

$$z \approx \frac{\langle U\rangle}{N} \tag{8}$$

The full description and derivation of the FENEX method can be found in the previous papers about the formation of compound phases[15,23,25] and relevant software is also available on our group GitHub page (github.com/escobedo-lab/FENEX). For every point along the estimated coexistence line estimated with the FENEX method, we conducted simulations that consisted of $3\times10^6$ MC cycles, with the first $10^6$ cycles used for equilibration. Additional cycles were carried out if there were large volume fluctuations during the simulation (signaling a lack of convergence or a tendency to a phase transition/inversion). Each cycle involved $N$ translation moves, $N/2$ rotational moves (for the polyhedra only), $N/5$ swap moves, and 3 volume attempts. For the octahedra+spheres system, the box shape was variable, allowing triclinic volume moves. To calculate $z$ in Eq. (7) when integrating over $\lambda$ or $\zeta$, we conducted one virtual move per MC cycle to change the size of the indentation or the sphere. Since errors accrue the farther one takes the integration from the original coexistence point, we conducted consistency checks by carrying out integrations following alternate paths (e.g., integrating first over energy and then over size ratio, or vice versa) which started and ended at the same set of conditions ($\lambda$, $\zeta$, $\varepsilon^*$). The average relative error in the end-point coexistence pressures found this way was ~ 10% or less.

The initial point to jump-start a coexistence line describing the effect of the non-convexity ratio was obtained from interfacial pining simulations for the flat-faced polyhedra and spheres system. We followed the iterative protocol laid out in Ref. [35] to obtain the coexistence pressure point (and associated coexistence phase densities). The order parameter chosen to pin the interfacial was the specific volume ($v$ = 1.81) and the initial guess for the coexistence pressure was set to $p$ = 8.02; the volumes of the crystalline and isotropic phases were retrieved as described in Ref. [24]. The overall system consisted of 2196 particles, the original box shape had an elongated shape (~2.5:1

aspect ratio) to accommodate bulk-like regions of both phases, and the pinning spring constant was set to 1800 $L^3/\beta$. Typically, 4-5 iterations were needed to attain convergence in pressure.

In analogy to systems of large + small hard spheres that form the NaCl solid,[36] we expect that for the athermal system of flat smaller cubes and larger spheres, the associated NaCl phase (if attainable) upon decompression would continuously transition into an interstitial solid solution (ISS) as the number of cubes decreases from the stoichiometric composition while being in equilibrium with an isotropic phase of nearly pure cubes. To approximately map this NaCl-to-ISS transition pressure, we used the following protocol:

1. Simulate the crystalline phase at equimolar composition for a given $P$.
2. Create an elongated box along the z axis containing the crystalline phase from step 1 and an isotropic phase of small cubes that share the cross section from step 1. The box contained 5184 particles, of which 2736 were in the NaCl phase (cubes and spheres) and 2448 were cubes in the isotropic phase at their initial state. The global number fraction of cubes was equal to 0.74.
3. Simulate the box from step 2 in the $NP_zT$ ensemble at the same given $P$ (where $L_x = L_y$ remain fixed). Translation moves for the small cubes were treated separately from those for the large spheres. Cubes had two types of translational moves: aggressive moves with a large step size fixed at to ¼ $L_x$ (to allow cubes to hop over across interstitial spots) and milder moves (to allow local equilibration) where the step size was chosen to keep the acceptance ratio ~ 10%. For the translation moves of the spheres, the acceptance ratio was kept at 30%. We also used strip volume moves[37] along the box's z axis to help volume equilibration of larger boxes.

4. Calculate the fraction of the interstices ($x_i$) between the spheres in the crystalline phase that are filled with cubes, noting that $x_i \approx 1$ in the NaCl phase and $x_i < 1$ in the ISS.
5. Repeat steps 1-4 until finding the smallest pressure for which the $x_i \approx 1$ is found.

After completing the simulations, we calculated several order parameters (OPs) to characterize the crystalline phase. The average cubatic orientational order parameter $P_4$ was found from: [38]

$$P_4 = \frac{1}{14N_2}\sum_{ij} 35\left|\boldsymbol{u}_{ij}\cdot\boldsymbol{n}\right|^4 - 30\left|\boldsymbol{u}_{ij}\cdot\boldsymbol{n}\right|^2 + 3 \tag{9}$$

where $N_2$ is the number of cubes, $\boldsymbol{u}_{ij}$ is the unit vector of particle $i$ along its axis $j$, and $\mathbf{n}$ is the unit vector that maximizes $P_4$. We determined if the C* phase maintained the expected substitutional order of the compound phase through the short-range compositional order parameter (SROP):[39]

$$\text{SROP} = \frac{1}{N}\sum_i \frac{t_i}{N_n} \tag{10}$$

Here, $N_n$ is the number of unlike nearest neighbors of a given particle in the compound phase, which is equal to eight for CsCl and six for NaCl. $t_i$ is the number of different-species neighbors of particle $i$ among its $N_n$ closest neighbors.

We quantified the extent of NP fluctuations in the C* phase to evaluate the effect of the indentations on local mobility. NVT simulations were carried out at the density corresponding to the C* phase at equilibrium with the I phase with $N$ translation and $N/2$ rotational moves with high acceptance probabilities (between 75% and 95%) and without swap moves to mimic pseudo-diffusive particle dynamics.[40,41] Unwrapped coordinates were stored every $10^3$ MC cycles to calculate the mean square displacement as a function of the MC cycles ($\Delta C_t$):

$$RMSD_t = \sqrt{\frac{\sum_{i=1}^{N}\sum_{j=0}^{N_{MC}-\Delta C_t}\left|r_{t+j}^{i} - r_j^{i}\right|^2}{N(N_{MC}-\Delta C_t)}} \tag{11}$$

where $N_{MC}$ is the total number of MC cycles and $r$ is the center of mass of the particle. A correction for the whole-system drift was accounted for by subtracting $\left|r_{t+j}^{average} - r_j^{average}\right|^2$ from every particle.

## 3. RESULTS

### 3.1. Non-additivity Parameter Calculation for Flat Polyhedra+Spheres

A system is considered to have a negative non-additive volume of mixing if $\Delta v < 0$. In the absence of indentations, non-additivity can be achieved when the spheres are larger than the polyhedra as shown in

Figure ***2***. We see that a more negative non-additivity value is achieved for the cubes+spheres case because the NaCl lattice is more amenable to accommodate the small cubes in the octahedral interstices between the spheres. For the CsCl system, the achievable negative non-additivity is very weak and occurs at a lower size ratio $\zeta = 1.19$. For size ratios greater than 6, the cubes in the NaCl phase start to lose orientational order and eventually reach a rotator-like state as seen by the drop in the $P_4$ parameter. A similar drop in the orientation order is also observed for the octahedra in the CsCl phase for large $\zeta$.

A high degree of negative non-additivity can be generally associated with conditions that are favorable for the stabilization of the compound phase C*, the reason is that at a high enough pressure $p_{hi}$ where incompressibility sets in, the likely phases competing with the C* phase are the

solid phases for the pure components which would be brought about by phase segregation. The Gibbs free energy change from the pure component to the C* state at those conditions is

$$\Delta G = p_{hi}(V^* - x_1 V_1 - x_2 V_2) + T(S^* - x_1 S_1 - x_2 S_2) \quad (12)$$

where $x_i$, $V_i$, and $S_i$ are the mole fraction, volume, and entropy of component $i$, and $V^*$ and $S^*$ are the volume and entropy of the C* phase. As a first approximation we could assume that particles are 'frozen' in their lattice structures (noting also that the C* lacks mixing entropy), so that entropies before and after compounding are comparable and small, and the entropy term in Eq. (12) can be neglected:

$$\Delta G \approx p_{hi}(V^* - x_1 V_1 - x_2 V_2) \propto \Delta v \quad (13)$$

Thus if $\Delta v < 0$, then $\Delta G < 0$, and the C* phase will be more stable than the phase-segregated state of the pure components' solid phases. This scenario should remain true for a range of $p < p_{hi}$ as long as the $S$ term remains small.

The above argument provides the basis for explaining the occurrence of the NaCl phase in other athermal systems with asymmetrically sized components. Indeed, Filion et. al. [36] found that mixtures of small and larger hard spheres with size ratios between 2.22 and 3.33 have noncongruent athermal behavior, where the athermal NaCl-lattice phase transitions first to an interstitial solid solution (ISS) at a fixed number of spheres and cubes. It can be shown that for such binary mixtures of hard spheres, the athermal NaCl phase can be stabilized in the region of component size ratios in which the corresponding $\Delta v < 0$.[25] Indeed, for the system of small and large spheres, the non-additivity parameter ranges from -0.02 to -0.047 in the size ratio range of $2.22 < \zeta < 3.33$ associated with the athermal NaCl crystallization, with a minimum of $\Delta v = -0.47$

for $\zeta \approx 2.75$ (see Fig. 2(a)). We also show below that a mixture of small cubes and large spheres expectedly exhibited a phase behavior similar to that of small + large spheres.

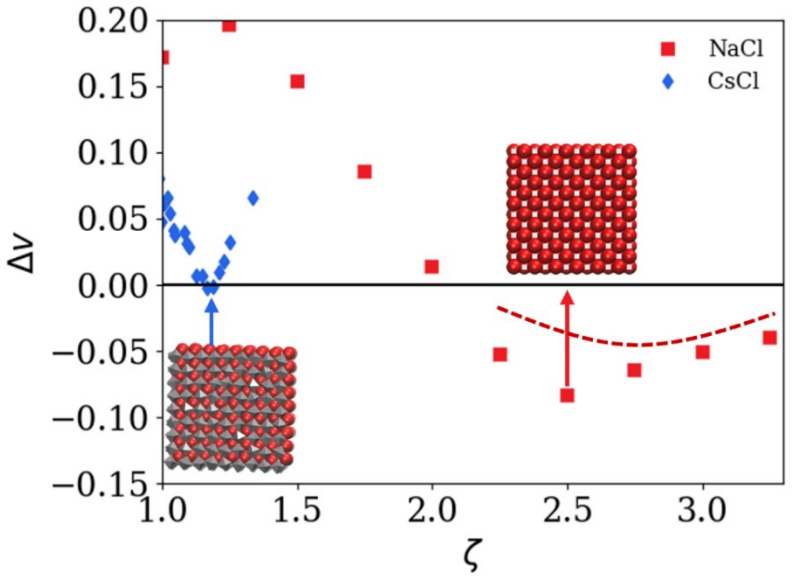


(a)

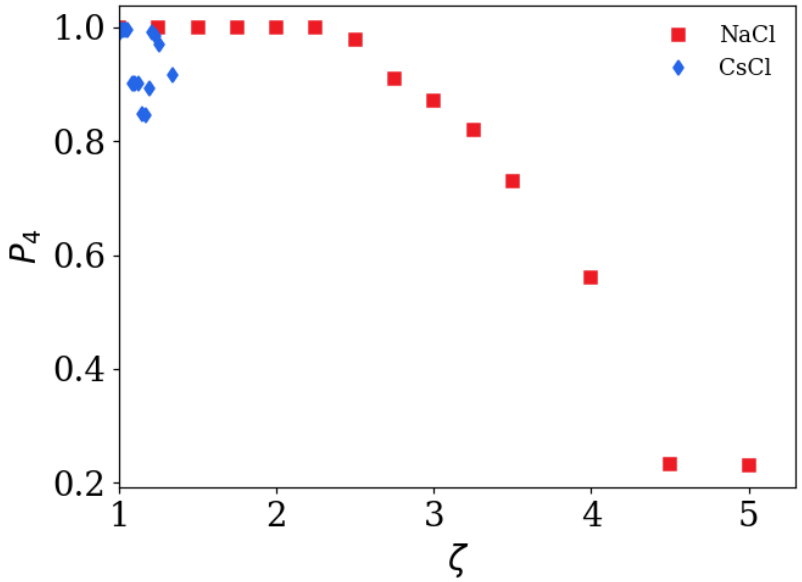


(b)

**Figure 2**: (a) Non-additive mixing parameter as defined in Eq. (5) as a function of $\zeta$ for $\lambda = 0$. Insets show the spheres+cubes NaCl phase (for $\zeta = 2.5$) and spheres+octahedra CsCl phase (for $\zeta = 1.19$) at their maximal negative non-additivity points. Red dashed line corresponds to NaCl phase

for equimolar large + small hard spheres. (b) Orientation order parameter ($P_4$) of the polyhedra in the crystalline C* phase as a function of the size ratio. Simulations were carried out at $P^*$=1000 and $\lambda = 0$.

The distinguishing features of the ISS phase are: (i) the non-fixed, lower than stoichiometric ratio of guest (small/'solute') component to host (larger/'solvent') component), which leaves empty some of the host crystal interstitial sites and, (ii) the usually weaker bonding and disparate size ratio between components which may allow the diffusion of guest particles through the network of empty interstitial lattice sites. While the ISS phase and the stoichiometric compound phase share the same underlying lattice geometry and could both be seen as being C* phases, in this paper we associate the C* phase specifically for the latter as this is the basis for the calculation of the non-additivity parameter $\Delta v$.

### 3.2 Non-additive phase behavior for small flat cubes and large spheres

As shown in

Figure ***2***, athermal mixtures of flat cubes and spheres with significantly unequal size ratios can lead to significant negative non-additivity.

To verify that the associated NaCl C* phase can be formed in such systems, we calculated the transition pressure between the ISS and the C* phase for the size ratio corresponding to the minimum value of $\Delta v$ using interfacial simulations. In Figure 3 we show the relationship between the pressure and the filling fraction $x_{filling}$ of the ISS phase. The filling fractions is defined as the ratio between the number of polyhedral in the C* phase and the maximum number of polyhedral in the C* phase. The smallest pressure for which $x_{filling} \approx 1$ corresponds to the transition pressure

between the NaCl and ISS phases (for convenience the threshold value to assign a NaCl character was set to $x_{filling}$ = 0.99). Note that $v_{C*}$ increases sharply as this transition point is approached because of the rapid loss of cubes in the C* phase. Congruent or incongruent athermal behavior with the flat octahedra+spheres was not achieved for the CsCl lattice, probably due to the low values of the non-additivity parameter for the CsCl. The NaCl lattice with octahedra + spheres transitioned into a disordered state even at high pressure and with energetic interactions between the sphere and the octahedra facet.

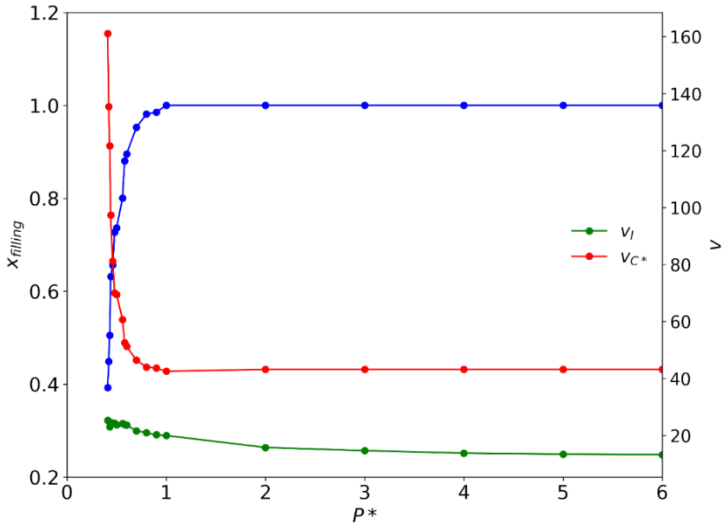


(a)

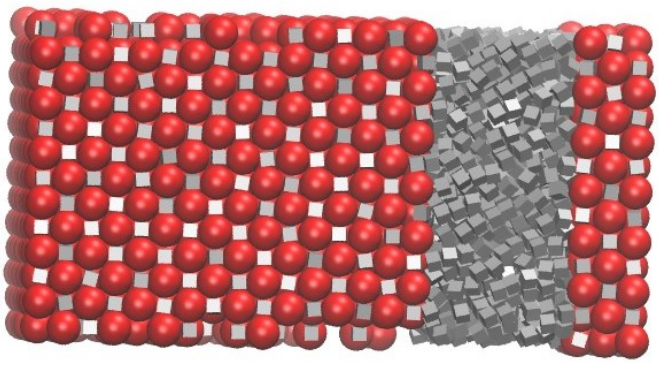

(b)

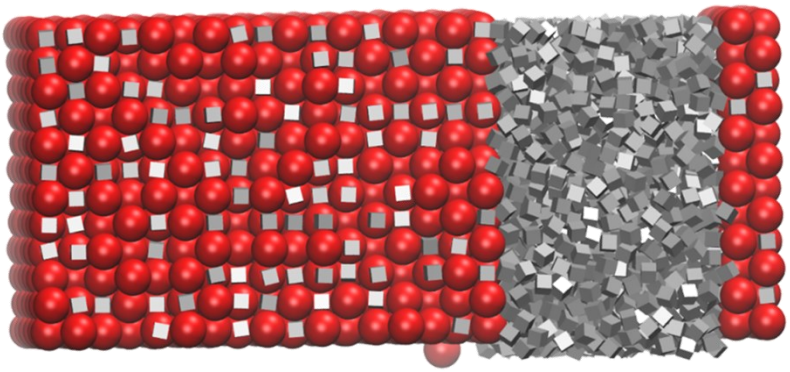

(c)

**Figure 3**: (a) Filling fraction ($x_{filling}$) of the cubes+sphere NaCl phase in equilibrium with a cubic isotropic phase in an interfacial simulation (blue line) and average volume per particle of the cube phase ($v_i$) and the C* phase ($v_{C*}$) as a function of pressure ($P^*$). Simulation done for $\zeta = 2.5$ and $\varepsilon^* = 0$. (b) Snapshots of the simulated interfacial system for $P^* = 0.8$ and $x_{filling} = 0.98$ and (c) $P^* = 0.5$ and $x_{filling} = 0.74$.

### 3.3 Non-additivity Parameter Calculation for Dented Polyhedra+Spheres

Figure 4 shows the relation between $\Delta v$ and $\lambda$ for both mixtures of polyhedra and spheres. It can be seen that compared to the octahedra+spheres mixture (which forms the CsCl phase for comparably sized components), the cubes+spheres mixture (which forms the NaCl phase) has a more positive value of the $\Delta v$ non-additivity parameter for the flat case but also a wider range of negative non-additivity values for large indentations. We attribute this difference to the geometric restriction on the maximum achievable indentation diameter for the octahedra+spheres system; while using smaller spheres would allow their deeper penetration into the dents and a more negative non-additivity, this can also causes the destabilization of the CsCl phase.[15,23] A similar destabilization of the C* phase occurs in the cubes+spheres mixtures for sufficiently low $\zeta$ and large $\lambda$, but the NaCl lattice can accommodate larger indentations (relative to the facet edge) for large $\zeta$. On the other hand, for larger size ratios the effects of the indentations on $\Delta v$ are small since

the spheres are too big to fit inside the facet dents. Although any indentation size can create an entropic polyhedron-sphere facet bonding effect, and octahedra indeed have more facets than cubes, our previous study on cubes showed that attaining significant negative non-additivity (as per $\Delta v$ values) is a good indicator that such a bonding effect will be sufficiently strong to stabilize the athermal C* phase.

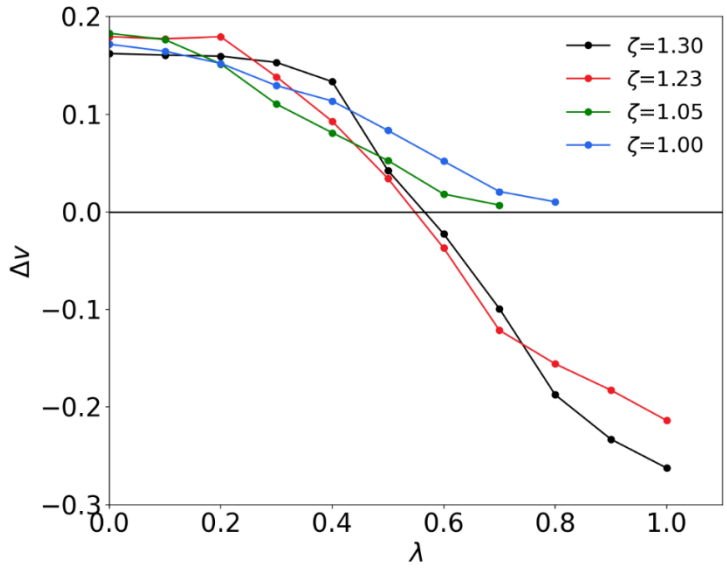


(a)

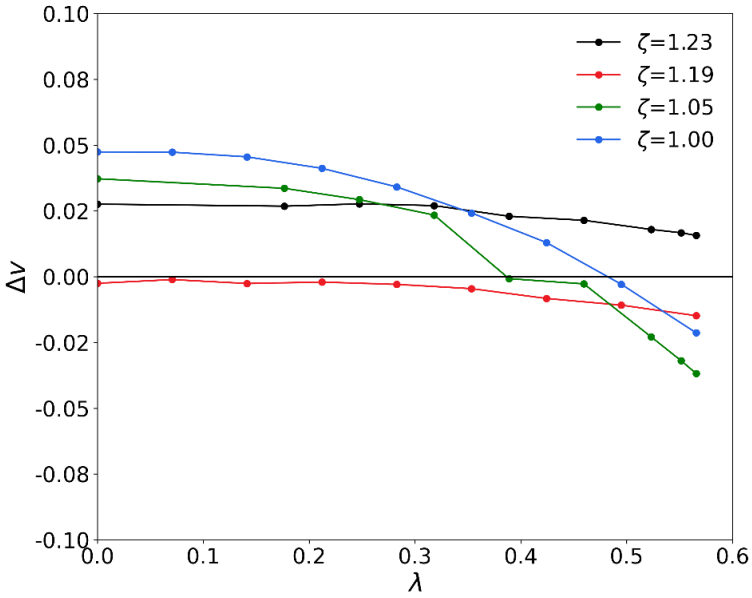


(b)

**Figure 4**: Non-additive mixing parameter as defined in Eq. (5) as a function of indentation ratio ($\lambda$) and different values of size ratio ($\zeta$) for (a) the NaCl phase of cubes+spheres and (b) the CsCl phase of octahedra+spheres.

### 3.4 Effect of indentation on the phase behavior of similarly sized components in octahedra + spheres mixture.

Given that only very small degrees of negative non-additivity is attainable for this system (as per Figs. 2 and 4), we started our exploration of the phase behavior with a system having sufficiently large energetic selectivity to ensure that a congruent transition to the CsCl phase was thermodynamically favored. Accordingly, we started the integration at the point corresponding to $\lambda = 0$, $\varepsilon^* = 1.15$, $\zeta = 1.00$, and $p = 7.15$, with properties obtained from an interfacial simulation. Initially, we integrated over changes on the indentation ratio ($\lambda$) and size ratio ($\zeta$) at fixed $\varepsilon^*$ to assess the effect of introducing the concavities on the octahedra's facets. Figure 5 shows the curves of coexistence pressure and (as inset) free energy ($\phi$) as a function of $\lambda$. For $\zeta = 1.23$, the variations in pressure and free-energy are negligible, indicating that the nestling of the relatively large spheres inside the small octahedra dents is minimal due to the limited accessible space created by the indentations. Additionally, for smaller $\zeta$, octahedra are larger than their lattice spacing so neighboring octahedra interact and can couple their positions and orientations while, in the larger $\zeta$ region, larger spheres prevent this type of interactions. Figure 6 shows the coexistence pressures and order parameters as a function of $\zeta$ for $\lambda$ = 0 and 0.57 and fixed energy parameter. There is a clear drop in the orientational order ($P_4$) and short-range compositional order (SROP) when the spheres are made bigger. Additionally, the plots show that the optimal $\zeta$ with regards to

the C* phase order parameter is higher for the indented octahedra when compared to the flat case ($\lambda = 0$), which was also observed for the cube + sphere system.[25] However, note that the increase in indentation leads to an increase in both coexistence $\phi$ and pressure, which is contrary to what was observed for the cubes + spheres system at any size ratio.[25] These $\phi$ values are readily available from the FENEX calculations and, according to the optimization rule advocated in Ref. [23], the more stable C* phase should be associated with lower $\phi$ values. The increase in $\phi$ can be partially explained by examining the terms contributing to the free energy as per Eq. (6). Figure 7(a) shows that for the cube-containing system the volume of the crystalline phase decreases at a faster rate with $\lambda$ than that for the isotropic phase, while for the octahedra-containing system, the difference in volume between the CsCl and I phases is smaller and largely insensitive to $\lambda$. (Note that the curves for the octahedra+sphere system stop at $\lambda = 0.57$ in Figure 7 as this corresponds to the maximum viable indentation). The derivative of the free energy for the indentation ratio, Eq. (7), also indicates that the indentations have a larger effect on the isotropic phase than on the crystalline phase (Figure 7(b)). Plots of how both the average volume and free-enery derivative $z$ change for the crystalline and isotropic phases are available in Figures S2 and S3 of the supplementary material. These two factors led to the increase in free energy with indentation size and to the conclusion that, at least for the conditions examined in Figs. 4 and 5, the introduction of indentations in the octahedra has a net destabilizing effect on the CsCl phase relative to the isotropic phase.

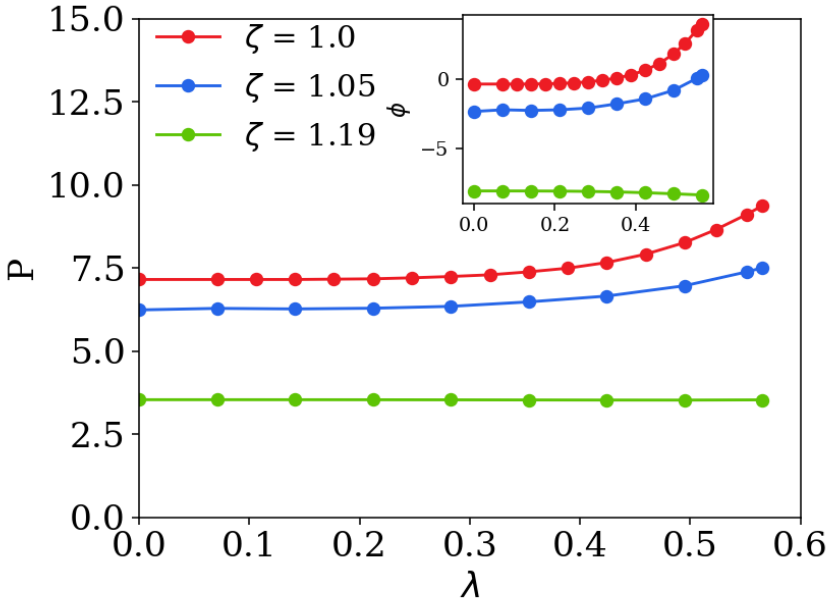


**Figure 5:** Coexistence pressure vs. indentation ratio ($\lambda$) of an equimolar mixture of octahedra + spheres for $\varepsilon^* = 1.1$ for different size ratios ($\zeta$). Inset shows how the relative coexistence free energy changes with indentation ratio ($\lambda$).

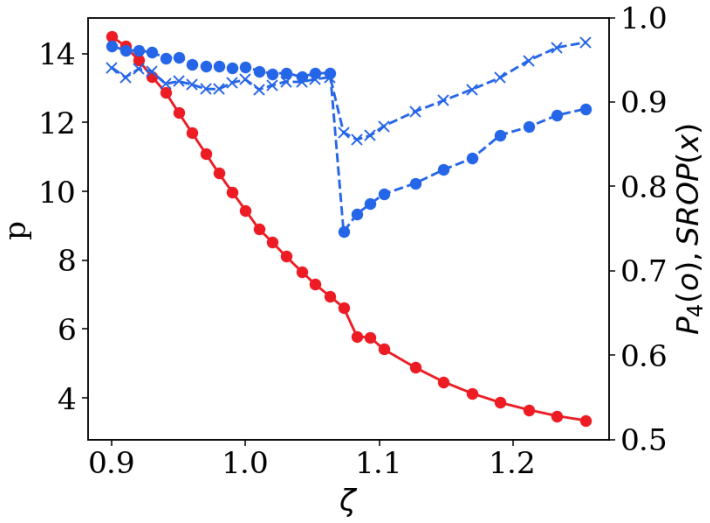


(a)

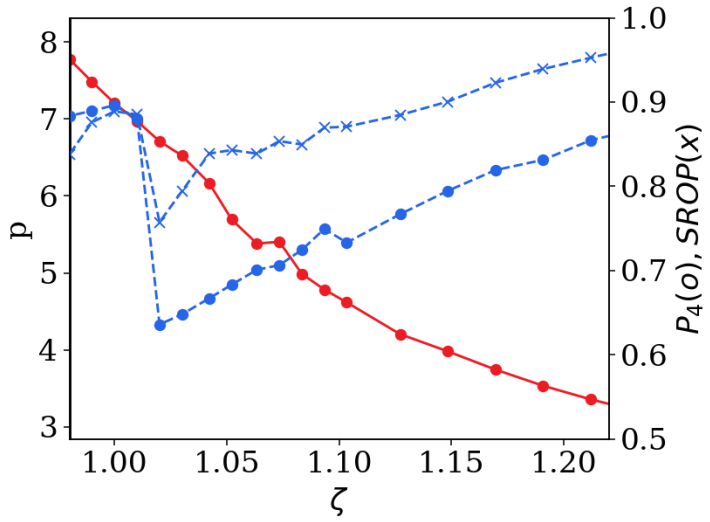


(b)

**Figure 6**: Coexistence pressure (red), orientation order parameter, $P_4$, (blue dots), and short-ranger order parameter, SROP, (blue crosses) vs. size ratio ($\zeta$) for the equimolar mixture of octahedra + spheres with $\varepsilon^* = 1.1$ and for (a) $\lambda = 0.57$, and (b) $\lambda = 0$.

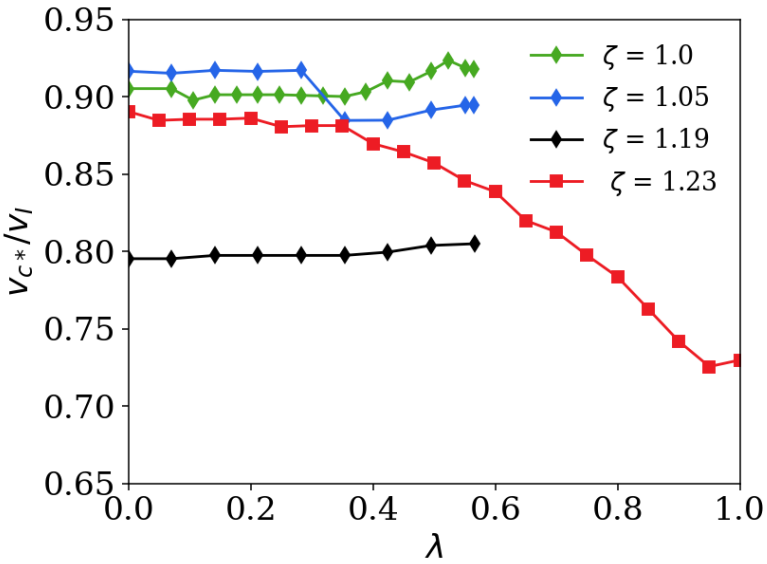


(a)

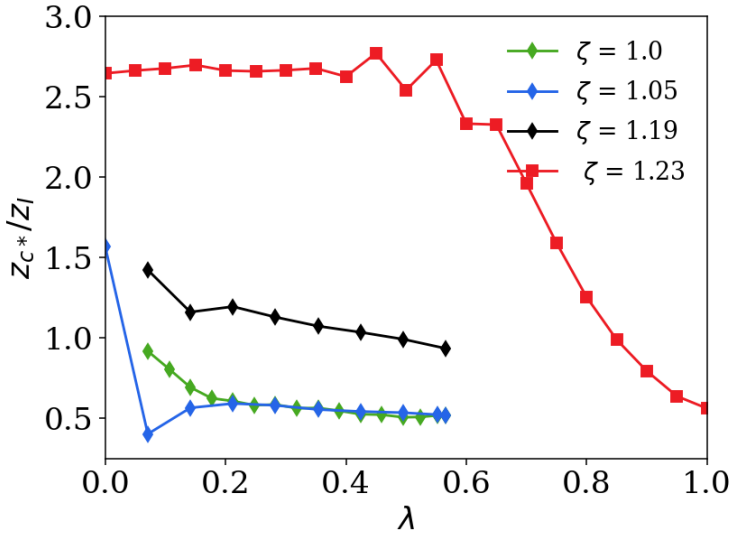


(b)

**Figure 7**: (a) Average volume ratio between the C* and I at equilibrium as a function of the indentation ratio ($\lambda$). (b) Average ratio of derivative $z$ of Eq. (7) between the C* and I phases at equilibrium as a function of the indentation ratio ($\lambda$). The lines correspond to: (-♦-) octahedra+ sphere mixture at $\varepsilon^* = 1.1$ and (-■-) cube+ sphere mixture at $\varepsilon^* = 0.55$.

### 3.5 Comparison between Octahedra+Spheres and Cubes+Spheres cases.

The most significant finding of our previous paper [25] on the cubes + spheres system was the discovery of a relatively large region in $\lambda - \zeta$ parameter space that resulted in an athermal I-C* congruent phase behavior. To find this region for the octahedra+sphere system, a thermal (non-zero $\varepsilon*$) initial point was chosen to start the integration for convenience. We then calculated the phase diagram for fixed values of $\zeta$ and $\lambda$ for varying values of the strength of the inter-species attraction energy parameter ($\varepsilon^*$). In Figure 8 (a), we highlight the region of the phase diagram where the athermal congruent I-C* phase transition was found for spheres+octahedra and spheres+cubes systems. In both cases, the actual athermal region (at finite pressures) is consistent with, but a subset of, the conditions where the non-additivity parameter (for infinite pressure) is negative in Figure 2, supporting the tenet that athermal congruent phase transition is largely driven by a decrease in the $pV$ term of the free energy. Note that athermal congruent behavior ($\varepsilon^* = 0$) for the C* phase formed by octahedra + spheres is only reached for the maximum value of the indentation size $\lambda = 0.57$ and a very narrow range of size ratios ($\zeta$) from 1.01 to 1.05. The athermal region for the octahedra+spheres system also coincided with the region with the highest structural order of the C* phase in Figure 6. More details about the relationship between $\lambda$ and the minimum values of $\varepsilon^*$ necessary to stabilize the C* phase are provided in the supplementary material.

Overall, the athermal region of the C* phase stability is significantly smaller for the octahedra+spheres system than that for the cubes + spheres system, which is attributed to the smaller $pV$ change in the octahedra+sphere system associated with the relatively smaller octahedron's facets and concomitant indentations achievable. That equimolar mixtures of spheres and cubes in a NaCl lattice arrangement are better at filling an available volume than equimolar mixtures of spheres and cubes in a CsCl lattice arrangement is well encapsulated by the difference

in magnitude of the non-additive parameter $\Delta v$ which acts as a surrogate of the C*-phase formation driving force: while both types of mixtures can achieve negative $\Delta v$ values, the former system can attain an order of magnitude larger negative $\Delta v$ values as illustrated for flat and dented polyhedra in Figs. 2(a) and 4 respectively.

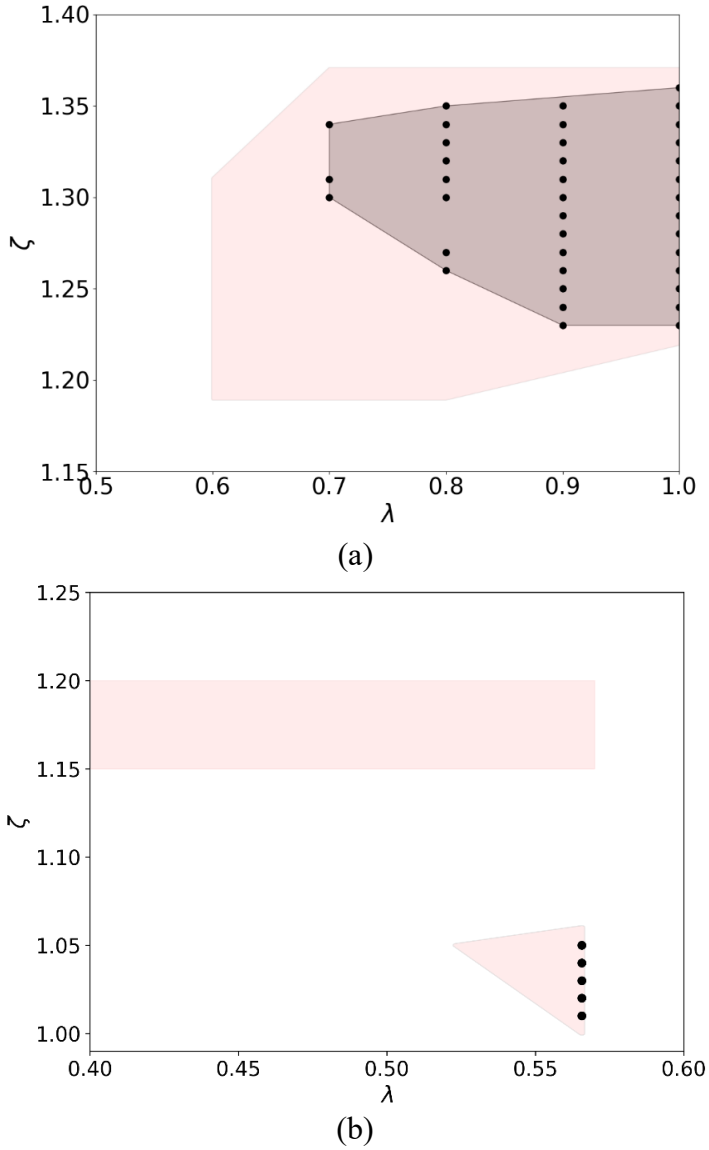


**Figure 8**: (a) ζ-λ region (shaded in gray and black dots) where athermal (ε* = 0) I-C* phase behavior occurred in our simulations for the (a) cubes+spheres system (b) octahedra+spheres system. The pink shaded region corresponds to negative values of non-additive mixing parameter $\Delta v$ calculated as per Eq. (5).

### 3.6 Driving forces for athermal congruent phase behavior

For the congruent phase transition from the isotropic to the C* phase one can write the change in the Gibbs free-energy ($G$) as:

$$\Delta G = \Delta U + p\Delta V - T\Delta S \tag{14}$$

where $U$ is potential energy and $\Delta$ refers to the change upon phase transition (C* minus isotropic). For the athermal systems, we can drop the $\Delta U$ term.

Our analysis of the cubes + spheres system showed that one of the major factors contributing to the athermal I-C* phase transition is the larger decrease in $pV$ term during the transition as the indentation ratio increased, as demonstrated in Figure 9(a) for the athermal system. This decrease helps to stabilize the crystalline phase as it tends to make $\Delta G$ more negative, thus counteracting the loss of entropy in the C* phase (i.e., from the loss of rotational entropy of the cubes and the loss of mixing entropy to create substitutional order). Indeed, at the athermal isotropic-C* phase coexistence point where $\Delta G = 0$, Eq. (14) shows that since $\Delta V < 0$ (and $\Delta U = 0$), then $\Delta S < 0$, i.e., the C* phase has expectedly less entropy than the isotropic phase. For the octahedra+spheres system, due to the restricted conditions where congruent transition occurs, we could not conduct a comparison of $pV$ values across indentation values for $\varepsilon^* = 0$. Hence, in Figure 9(b) we show the relationship between $pV$ and indentations for $\varepsilon^* = 1.1$. The decrease in $pV$ effect only happens for the size ratio where the athermal phase behavior was found as expected. However, it is unclear whether larger indentations may tend to increase the vibrational entropy of the C* lattice and hence help reduce the magnitude of $|\Delta S|$.[44] To probe this question, we monitored the root mean squared displacement (RMSD) of the species in the crystalline phases at coexistence. The particles' fluctuations from their respective lattice positions (as calculated through the MSD) can be seen as

quantifying the amplitude of particle vibrations and hence be a contributor to the total particle entropy (noting that, at thermal equilibrium between phases, any contribution from momenta or kinetic degrees of freedom cancel out in $\Delta S$).[42] In Figure 10, we display the RMSD displacement for the athermal NaCl phase of cubes+spheres at equilibrium for two indentation values. We observe that larger indentation slightly decreases the average RMSD, implying a decrease in vibrational entropy (with the lattice spacing remaining constant). We also made the same comparison for the octahedra + spheres CsCl phase, albeit we could not compare athermal systems because of the lack of a large athermal region for dented octahedra. Nevertheless, we detected the same trend of decreasing in vibrational entropy with indentation ratio, as shown in Fig. S5 of the supplementary material.

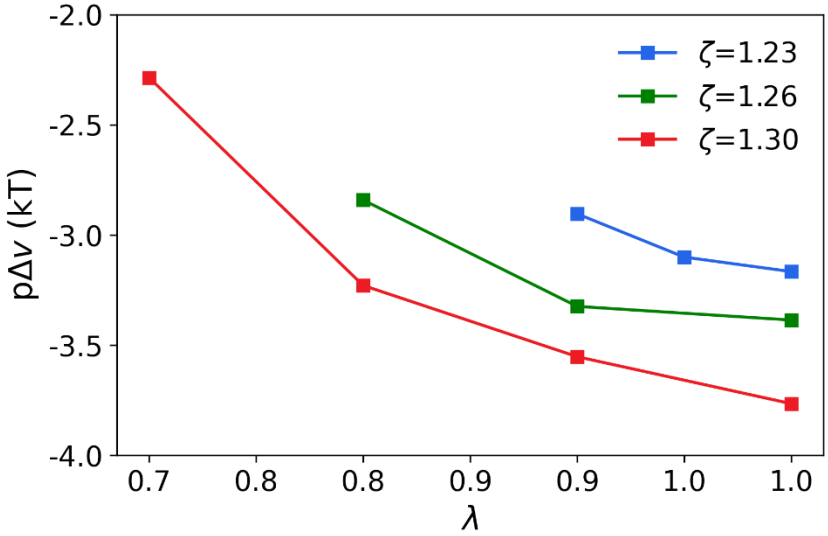


(a)

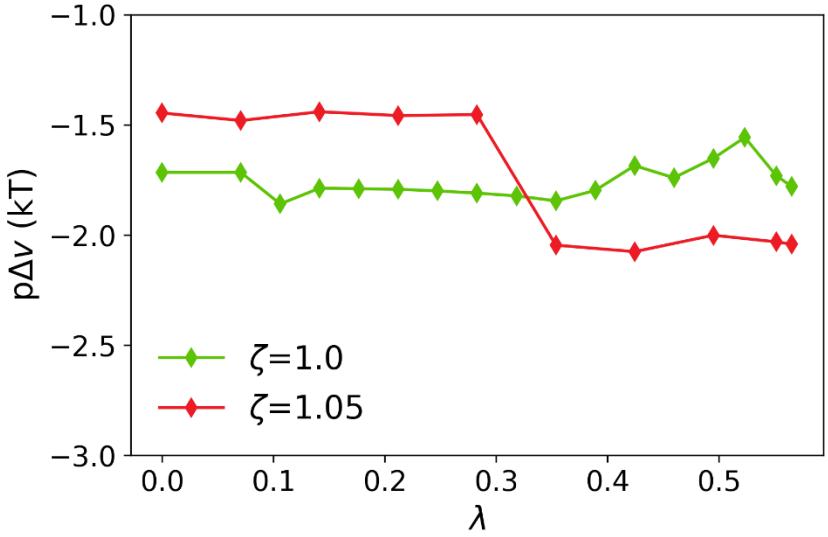


(b)

**Figure 9**: Difference in the reduced volume $p(v_{c*} - v_I)$ as a function of the indentation ratio ($\lambda$) and different size ratios ($\zeta$) at isotropic-C* phase coexistence for (a) the cubes +sphere system in the athermal region, (b) the octahedra +sphere system for $\varepsilon^* = 1.1$.

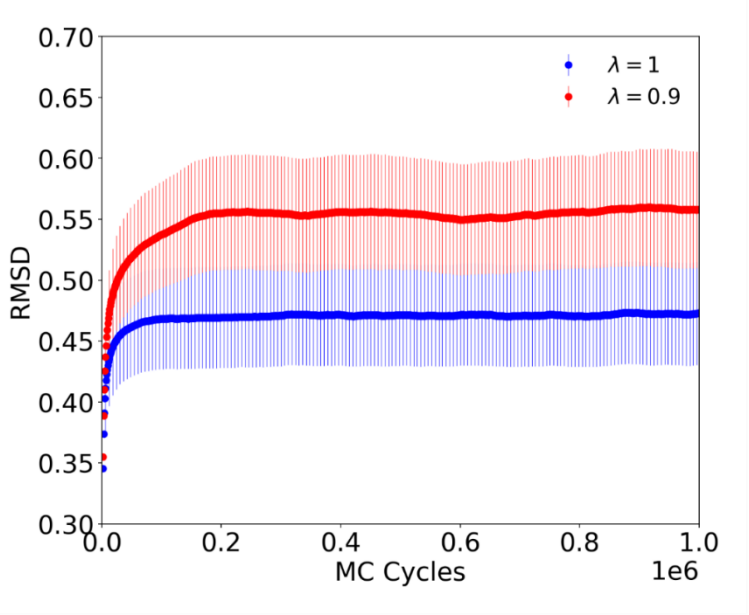


**Figure 10**: Average Mean squared displacement as a function of the MC cycles for the athermal NaCl phase. Size ratio was kept the same ($\zeta = 1.23$) for these plots and error bars appear as vertical lines.

The $pV$ effect caused by the indentations can be associated with the strengthening of the polyhedra-sphere entropic bonds and, in the athermal systems, an entropic bond that can be as strong as the energetic bond needed to stabilize the C* phase with flat polyhedra at conditions when it was otherwise unfeasible. Figure 11 shows that expectedly the average bond distance between the polyhedra and spheres is shorter for larger $\lambda$ (for fixed $\zeta$) due to the extent of sphere-dent nestling behavior which is what effectively leads to a more efficient packing and a larger $pV$ effect upon ordering (as quantified in Fig. 4a and Fig. 7). We can then associate stronger bonds with shorter interspecies bond lengths.

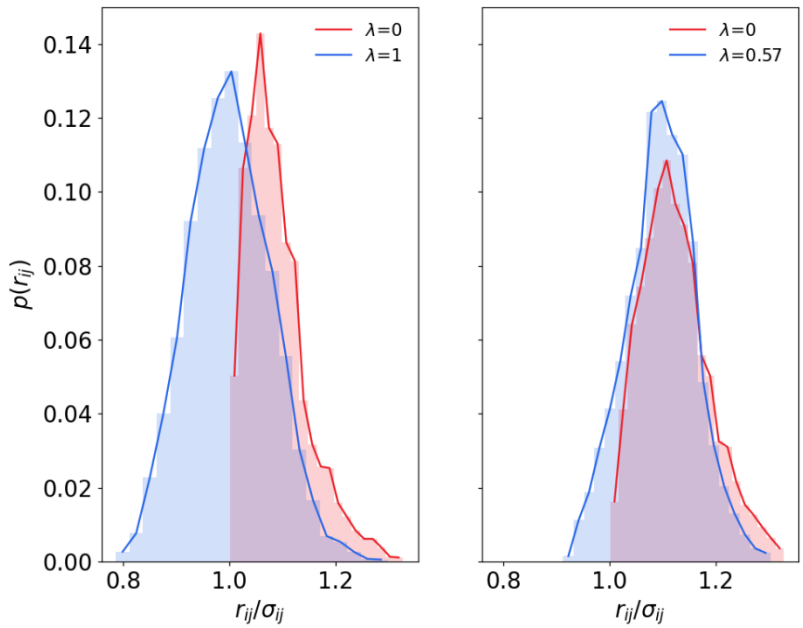


(a) (b)

**Figure 11**: Probability distributions of normalized bond length between spheres and polyhedra for two values of indentations in the crystalline phase at coexistence. The bond length is normalized by the contact distance between the center of the sphere and the center of a flat polyhedron ($\sigma_{ij}$) for (a) NaCl phase at $\varepsilon^*$ = 0.55 and $\sigma_{ij} = a/2 + \sigma/2 = 2.23$, and (b) CsCl phase at $\varepsilon^*$ = 1.1 and $\sigma_{ij} = h/2 + \sigma/2 = 1.41$.

## 4. CONCLUSIONS AND OUTLOOK

In this work we have examined how negative volumetric mixing non-additivity associated with the formation of the compound crystal from equimolar polyhedra+spheres binary mixtures can be generated by tuning the component size asymmetry and the presence of concavities in the polyhedra facets, and how such non-additivity correlates with the isotropic-crystalline athermal phase behavior, including congruent athermal crystallization. Two polyhedral shapes were

considered, cubes and octahedra, which when blended with spheres can form a crystalline compound C* with the NaCl and CsCl lattice, respectively.

First, we find that negative non-additivity (as quantified by our $\Delta v$ parameter) can be observed in mixtures of flat cubes and larger spheres, and that for relatively large spheres where $\Delta v < 0$, an athermal noncongruent isotropic-C* phase behavior ensues. This also demonstrates that it is the $pV$ contraction associated with the C*-phase formation (relative to the hypothetical competing state of segregated crystalline phases of the pure components) that is the main driving force that stabilizes such an athermal C* phase. While negative non-additive is also observed in mixtures of flat octahedra and spheres, this is very tenuous and restricted to a narrow range of component sizes; our simulations failed to any find finite-pressure conditions where the corresponding athermal C* phase was stable.

For the octahedra+spheres system, we used a specialized thermodynamic integration method to trace phase coexistence lines as a function of three main system variables, namely, the interspecies attraction strength, indentation ratio, and size ratio. Our findings suggest that the effect of facet indentations was not very beneficial in this case; specifically, increasing indentation led to higher coexistence free energy and pressure in the octahedra + spheres system. These trends contrasted with those observed in the cubes and spheres system at any size ratio. Furthermore, the athermal region for the octahedra+spheres system was limited to $\lambda = 0.57$ and size ratios ranging from 1.01 to 1.05 while a broader $\zeta$-$\lambda$ region was observed in our previous study of cubes+spheres. We also found that the reduction in the $pV$ term of the C* phase free energy resulting from the addition of indentations is the main force driving the athermal congruent phase transition and that this decrease, being smaller for the octahedra+spheres system, is responsible for the observed differences across systems. Our study also revealed that the presence of indentations slightly

decreases the particle vibrational entropy. However, this effect is compensated for by the gains associated with the strengthening of the entropic bonds.

We note that *effective* athermal, non-additive interactions can be abstracted even when ordering is aided by underlying anisotropic energetic interactions and external fields. One relevant example occurs in the self-assembly of binary systems of spherical colloidal particles into quasi-2D superlattices at a fluid-fluid interface.[43,44] In such a case, the components' centers of mass occupy different planes due to differences in how the two species interact with the two fluids, leading to rather unique superlattices. Such a system could be "coarse-grained" into a 2D binary mixture of "non-additive" co-planar hard disks where some overlap is only allowed between disks of unlike species.[43,44]

Overall, our findings provide specific ranges for the geometric parameters related to indentation and component sizes that drive the athermal phase ordering behavior of particles and form the basis for ongoing work. The impact of negative non-additive mixing on phase transition kinetics can also be studied via molecular simulations, as we previously demonstrated with a system of patchy particles having positive non-additivity.[45] Besides the geometry of the system, the relationship between the valence of the polyhedra particles and the indentation ratio can be explored further in simulations with other polyhedra particles of varying valence such as tetrahedral and dodecahedral frames. [27,32] A general question that we are expecting to address is: Can we use $\Delta v$ calculations to predict the favorable assembly of hard small polyhedra (flat or dented) + large spheres into a "$A_mB_n$" lattice, for any polyhedra shape and for any lattice compound $A_mB_n$ (where m/n indicate different stoichiometry)? Additionally, one could investigate the effects of size polydispersity [23,46] and the strength of the entropic bonds on the phase behavior and mechanical strength of these materials. Note that even pure component systems (where each

particle exhibits convex and concave regions) can also exhibit different ordered phases realizing varying degrees of nonaditivity.[47-48] In summary, our findings provide insights into how designing particle shapes that partially relieve geometrical frustration to attain denser structural packings can aid in the stabilization of compound crystals and can thus inform the design of new materials.

## ACKNOWLEDGMENTS

Funding support from NSF awards No. CHE-2101829 and CBET-2402416 are gratefully acknowledged. Support to I. Q. M. from the 2021 MolSSI Fellowship and to F. A. E. from grant NSF PHY-1748958 to the Kavli Institute for Theoretical Physics (KITP) are also acknowledged. F. A. E. is grateful to Prof. A. Travesset for insightful exchanges and I.Q.M. is grateful to Prajwal B. Bangalore and Dr. Abhishek K. Sharma for sharing insights into overlap codes implementation and fruitful discussions.

## SUPPLEMENTARY MATERIAL

See supplementary material for plots on the relationship between the minimum $\varepsilon^*$ for different $\lambda$ and vibrational entropy for the octahedra spheres system.

### Author contributions

**Isabela Quintela Matos**: Formal analysis (lead); Investigation (lead); Methodology (equal); Software (lead); Writing – original draft (lead). **Fernando A. Escobedo**: Conceptualization (lead); Funding acquisition (lead); Investigation (equal); Methodology (equal); Supervision (lead); Writing – review & editing (lead).

**Conflicts of interest**

The authors declare no conflicts of interest.

**Statement of Data Availability**:

The data that support the findings of this study are available from the corresponding author upon reasonable request.

## REFERENCES


1. E.C.M. Vermolen, A. Kuijk, L.C. Filion, M. Hermes, J.H.J. Thijssen, M. Dijkstra, and A. van Blaaderen, Proc. Natl. Acad. Sci. U. S. A. **106**, 16063 (2009).
2. X.W. Lou, C. Yuan, Q. Zhang, and L.A. Archer, Angew. Chem., Int. Ed. **45**, 3825 (2006).
3. C. Salzemann, I. Lisiecki, A. Brioude, J. Urban, and M.P. Pileni, J. Phys. Chem. B **108**, 13242 (2004).
4. S.J. Oh, N.E. Berry, J.H. Choi, E.A. Gaulding, H. Lin, T. Paik, B.T. Diroll, S. Muramoto, C.B. Murray, and C.R. Kagan, Nano Lett. **14**, 1559 (2014).
5. K. Deng, Z. Luo, L. Tan, and Z. Quan, Chem. Soc. Rev. **49**, 6002 (2020).
6. Z. Liu, X. Qin, Q. Chen, T. Jiang, Q. Chen, and X. Liu, Adv. Mater. **35**, 2209279 (2023).
7. I. Cherniukh, G. Rainò, T. Stöferle, M. Burian, A. Travesset, D. Naumenko, H. Amenitsch, R. Erni, R.F. Mahrt, M.I. Bodnarchuk, and M.V. Kovalenko, Nature **593**, 535 (2021).
8. Z.W. Li, Y.W. Sun, Y.H. Wang, Y.L. Zhu, Z.Y. Lu, and Z.Y. Sun, J. Phys. Chem. Lett. **12**, 7159 (2021).
9. F.X. Redl, K.S. Cho, C.B. Murray, and S. O'Brien, Nature **423**, 968 (2003).
10. X. Ye, J. Chen, and C.B. Murray, J. Am. Chem. Soc. **133**, 2613 (2011).
11. F. Lu, K.G. Yager, Y. Zhang, H. Xin, and O. Gang, Nat. Commun. **6**, 6912 (2015).
12. Z. Fan, and M. Grünwald, J. Am. Chem. Soc. **141**, 1980 (2019).
13. W.H. Evers, B. De Nijs, L. Filion, S. Castillo, M. Dijkstra, and D. Vanmaekelbergh, Nano Lett. **10**, 4235 (2010).
14. Y. Geng, G. Van Anders, P.M. Dodd, J. Dshemuchadse, and S.C. Glotzer, Sci. Adv. **5**, eaaw0514 (2019).
15. F.A. Escobedo, J. Chem. Phys. **146**, 134508 (2017).
16. M.I. Bodnarchuk, M.V. Kovalenko, W. Heiss, and D.V. Talapin, J. Am. Chem. Soc. **132**, 11967 (2010).
17. S. Sacanna, W.T.M. Irvine, P.M. Chaikin, and D.J. Pine, Nature **464**, 575 (2010).

18. M. Marechal, R.J. Kortschot, A.F. Demirörs, A. Imhof, and M. Dijkstra, Nano Lett. **10**, 1907 (2010).
19. G. Odriozola, and M. Lozada-Cassou, J. Phys. Chem. B **120**, 5966 (2016).
20. S. Asakura, and F. Oosawa, J. Chem. Phys. **22**, 1255 (1954).
21. A. Kumar, and V. Molinero, J. Phys. Chem. Lett. **8**, 5053 (2017).
22. S. Punnathanam, and P.A. Monson, J. Chem. Phys. **125**, 024508 (2006).
23. F.A. Escobedo, J. Chem. Phys. **140**, 094102 (2014).
24. F.A. Escobedo, J. Chem. Phys. **147**, 214106 (2017).
25. I. Quintela Matos, and F.A. Escobedo, J. Chem. Phys. **153**, 214107 (2020).
26. Y. Wang, J.T. McGinley, and J.C. Crocker, Langmuir **33**, 3080 (2017).
27. X. Huang, L. Song, X. Jiang, and X. Zhang, J. Mater. Sci. **57**, 7400 (2022).
28. K. Kadowaki, H. Ishii, D. Nagao, and M. Konno, Langmuir **32**, 11600 (2016).
29. C.W. Yang, K. Chanda, P.H. Lin, Y.N. Wang, C.W. Liao, and M.H. Huang, J. Am. Chem. Soc. **133**, 19993 (2011).
30. H. Zhang, Y. Lu, H. Liu, and J. Fang, Nanoscale **7**, 11591 (2015).
31. Y. Tian, Y. Zhang, T. Wang, H.L. Xin, H. Li, and O. Gang, Nat. Mater. **15**, 654 (2016).
32. K. Ma, Y. Gong, T. Aubert, M.Z. Turker, T. Kao, P.C. Doerschuk, and U. Wiesner, Nature **558**, 577 (2018).
33. A.S. Glassner, Graphics Gems (Academic Press, USA, 1990).
34. S. Gottschalk, M.C. Lin, and D. Manocha, in SIGGRAPH 1996 (Association for Computing Machinery, 1996), pp. 171–180.
35. V. Thapar, and F.A. Escobedo, J. Chem. Phys. **141**, 124117 (2014).
36. L. Filion, M. Hermes, R. Ni, E.C.M. Vermolen, A. Kuijk, C.G. Christova, J.C.P. Stiefelhagen, T. Vissers, A. van Blaaderen, and M. Dijkstra, Phys. Rev. Lett. **107**, 168302 (2011).
37. F.A. Escobedo, and Z. Chen, J. Chem. Phys. **121**, 11463 (2004).
38. B.S. John, C. Juhlin, and F.A. Escobedo, J. Chem. Phys. **128**, 041103 (2008).
39. Y. Xiong, Y. Yang, H. Joress, E. Padgett, U. Gupta, V. Yarlagadda, D.N. Agyeman-Budu, X. Huang, T.E. Moylan, R. Zeng, A. Kongkanand, F.A. Escobedo, J.D. Brock, F.J. DiSalvo, D.A. Muller, and H.D. Abruña, Proc. Natl. Acad. Sci. U. S. A. **116**, 1974 (2019).
40. F. Romano, C. De Michele, D. Marenduzzo, and E. Sanz, J. Chem. Phys. **135**, 124106 (2011).
41. B.P. Prajwal, J.Y. Huang, M. Ramaswamy, A.D. Stroock, T. Hanrath, I. Cohen, and F.A. Escobedo, J. Colloid Interface Sci. **607**, 1478 (2022).
42. B. Fultz, Prog. Mater. Sci. **55**, 247 (2010).
43. E. Fayen, A. Jagannathan, G. Foffi, and F. Smallenburg, J. Chem. Phys. **152**, 204901 (2020).
44. Y. Zhou, and G. Arya, Nat. Commun. **13**, 7976 (2022).
45. I. Quintela Matos, and F.A. Escobedo, J. Phys. Chem. B **127**, 3746 (2023).
46. F.A. Escobedo, J. Chem. Phys. **110**, 11999 (1999).
47. C. Avendaño, G. Jackson, E.A. Müller, and F.A. Escobedo, Proc. Natl. Acad. Sci. U. S. A. **113**, 9699 (2016).
48. C. Avendaño, and F.A. Escobedo, J. Chem. Phys. **129**, 174107 (2008).